PAPER • OPEN ACCESS

Overview of the hydraulic characteristics of the ITER Central Solenoid Model Coil conductors after 15 years of test campaigns

To cite this article: A Brighenti *et al* 2017 *IOP Conf. Ser.: Mater. Sci. Eng.* **278** 012178

View the article online for updates and enhancements.

Overview of the hydraulic characteristics of the ITER Central Solenoid Model Coil conductors after 15 years of test campaigns

A Brighenti[1], R Bonifetto[1], T Isono[2], K Kawano[2], G Russo[1], L Savoldi[1] and R Zanino[1]

[1] NEMO Group, Dipartimento Energia, Politecnico di Torino, Turin, Italy
[2] National Institutes for Quantum and Radiological Science and Technology, Naka, Japan

E-mail: laura.savoldi@polito.it

Abstract. The ITER Central Solenoid Model Coil (CSMC) is a superconducting magnet, layer-wound two-in-hand using Nb_3Sn cable-in-conduit conductors (CICCs) with the central channel typical of ITER magnets, cooled with supercritical He (SHe) at ~4.5 K and 0.5 MPa, operating for approximately 15 years at the National Institutes for Quantum and Radiological Science and Technology in Naka, Japan. The aim of this work is to give an overview of the issues related to the hydraulic performance of the three different CICCs used in the CSMC based on the extensive experimental database put together during the past 15 years. The measured hydraulic characteristics are compared for the different test campaigns and compared also to those coming from the tests of short conductor samples when available. It is shown that the hydraulic performance of the CSMC conductors did not change significantly in the sequence of test campaigns with more than 50 cycles up to 46 kA and 8 cooldown/warmup cycles from 300 K to 4.5 K. The capability of the correlations typically used to predict the friction factor of the SHe for the design and analysis of ITER-like CICCs is also shown.

1. Introduction

In the field of large-scale application of superconducting magnets, it is helpful to have a clear understanding of the hydraulic behavior of the conductors [1], [2] with the aim of minimizing, during the design phase, the pressure loss along the conductor and properly sizing the cold circulator. Moreover, the hydraulic characteristic of the conductors plays a significant role during off-normal transients, such as a quench event, in determining the quench propagation speed along the conductor. For the ITER magnet system, the fully superconducting Central Solenoid Model Coil (CSMC) [3], see figure 1a, a solenoid in operation since 2000 at the National Institutes for Quantum and Radiological Science and Technology (former JAEA) plays a relevant role in the related R&D as it is the only facility worldwide allowing the test of full-length ITER conductors in a background field up to 13 T. Since its commissioning, more than 15 years ago, the CSMC has operated several times during the test campaigns of the ITER Insert Coils, tested in the bore of the CSMC in 2000, 2001, 2002, 2004, 2015 and 2016-17, respectively.

The CSMC is constituted by 18 two-in-hands-wound layers, cooled by supercritical helium (SHe) at 4.5 K and 0.6 MPa in nominal conditions. Slightly different Cable-in-Conduit Conductors (CICCs) were used for different layers (two different void fractions in the bundle region and, for one of the two, spiral versus coiled wire used for the central channel) so that three groups of hydraulically similar conductors can be clearly identified on the basis of the conductor geometry. Six (out of the 36)

conductors, representative of those three groups, are instrumented with differential pressure measurement and flow meters so their hydraulic characteristics can be directly measured. A very detailed analysis of the hydraulic characteristics of the different conductors, some of which were already investigated on dedicated experiments on short lengths [4], was performed just after the first test campaign, deriving ad-hoc correlations for the friction factors [5], but they were never rechecked with the same level of detail for the following campaigns.

During the different test campaigns, the CSMC underwent 50+ full charges (up to 46 kA, resulting in a magnetic self-field of 13 T), 10+ fast current discharges from full power, 200+ fast discharges from ~10 kA current (the so-called "daily checks"), 6 quenches in layer #1A and 8 cooldowns from room temperature to cryogenic temperature. As some of the tested Insert Coils, having a void-fraction comparable to that of the CSMC conductors, showed some effects of the Lorentz forces on the pressure drop along the conductor [6], the aim here is to check that no permanent variation of the hydraulic characteristics took place in the 15-years operation of the magnet. The wide dataset is then used to assess the accuracy of available correlations, largely used nowadays in computing the pressure drop along the conductors for, e.g., the assessment of the ITER operating scenarios, as well as for the design of CICCs for, e.g., future DEMO tokamaks.
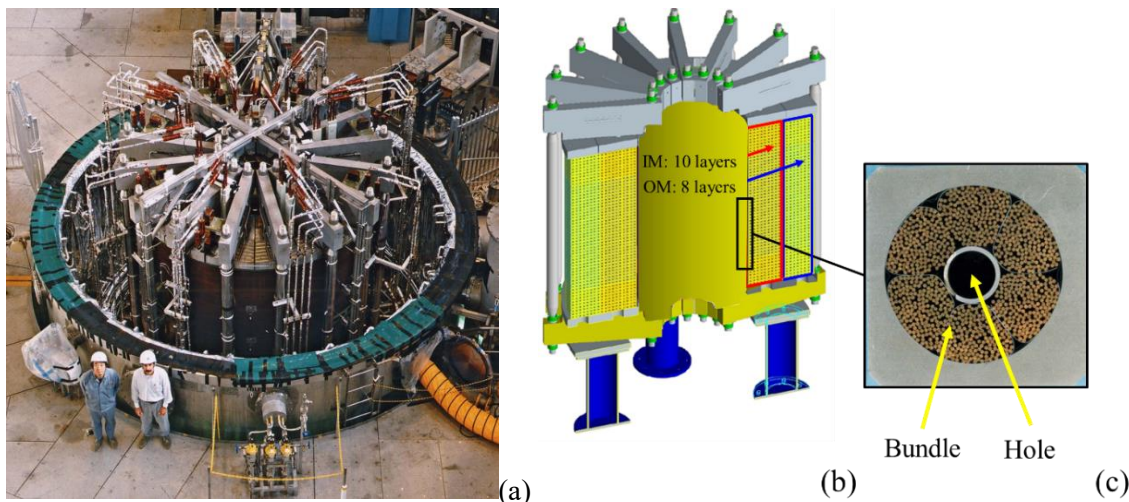
Figure 1. (a) Open cryostat of the CSMC facility @ National Institutes for Quantum and Radiological Science and Technology at Naka, Japan (courtesy of QST). (b) Cross section of the CSMC showing the IM and OM. The inset (c) shows one of the CICC used for the ITER CSMC (courtesy of QST).

2. CSMC layout
The 18 layers of the CSMC are organized in two modules: Inner Module (IM, layers #1-10) and Outer Module (OM, layers #11-18), see figure 1b. Each layer consists of 15 to 17 turns (for the first four layers and the remaining ones, respectively). All the conductors have a central cooling channel, see figure 1c, and a bundle of Nb_3Sn superconducting strands. The geometrical parameters relevant for the pressure loss calculation along the different conductors are reported in Table 1. Note that the geometry of the hole is the same for conductor 1A (i.e. from 1A to 4B), 9A-10B and OM (i.e. 11A-18B), while the bundle hydraulic diameter of conductors 5A, 7A (i.e. from 5A to 8B), 9A-10B and OM is the same. The conductors equipped with differential pressure taps, flow meters, inlet and outlet temperature sensors and pressure tap, see figure 2, for which the hydraulic characterization is thus possible, are:

- Conductor 1A, which is fully representative of all the CICCs in the first four layers (1A-4B), with the central channel delimited by a flat spiral, manufactured in the US;
- Conductors 5A and 7A, which are fully representative of the CICCs in layers 5A-8B with the central channel delimited by a spring, manufactured in the US;

- Conductors 11A, 15A and 17A, which are representative of the CICCs of the two outermost layers of the IM (9A-10B) and of the entire OM (11A-18B), again with the central channel delimited by the flat spiral, manufactured in Japan (except layer #17, manufactured in the US).

Table 1. Geometrical parameters of the conductors in the two modules of the CSMC.

|	Units	IM		OM
		1A	*5A and 7A*	*11A, 15A and 17A*
Number of strands	[-]	1152	1080	1080
Strand diameter	[mm]	0.81	0.81	0.81
Bundle void fraction (φ)	[%]	36.3	35.8	35.8
Strand twist pitch angle ($\cos\theta$)	[-]	0.931	0.967	0.967
Internal hole diameter (D_h)	[mm]	10.0	9.0	10.0
Spiral/spring thickness and width (h)	[mm]	1.0/3.0	1.5/1.5	1.0/3.0
Length (L)	[m]	84.9	117.9 /129.1	153.6 / 176.8 / 188.9
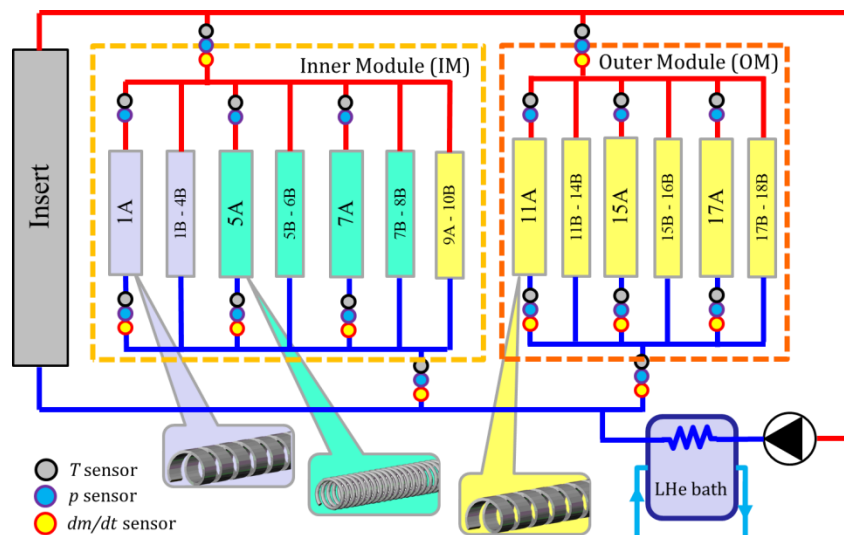
Figure 2. Sketch of the circuit diagram for the CSMC showing also which conductors have a flat spiral or a spring delimiting the central channel.

Data collected during cold operation in all the campaigns so far have been analyzed to find time frames in which the relevant thermal-hydraulic and physical quantities are constant for at least a mean residence time in the coil (the velocity in the bundle, the slowest path for SHe flow, is around 0.2 m/s in nominal conditions and by considering the longest outermost conductor 18A, the mean residence time is ~1000 s). The time average of the mean inlet/outlet temperature (T), mean inlet/outlet pressure (p), inlet mass flow rate (dm/dt) and pressure drop (Δp) have been then calculated for all the instrumented conductors. The gravity head contribution has been removed from the measured value of pressure drop, accounting for an effective height (vertical distance between the two taps of the differential pressure sensor) of ~5.3 m and evaluating the SHe density at thermodynamic conditions averaged between inlet and outlet.

3. Analysis of experimental data
The hydraulic characteristic, in terms of pressure gradient vs. total mass flow rate, is reported in figure 3 for the instrumented conductors for points at the nominal operating conditions of 4.5 K and 0.6 MPa at the coil inlet. Figure 3 shows that the collected points lay on the same trend line for all the

experimental campaigns, with the exception of a cluster of points measured during the 2008 campaign in conductors 5A and 17A, possibly indicating some issues in the flow measurement in that specific campaign. From this picture it is possible to conclude that the overall hydraulic characteristic of the different conductors has remained basically the same throughout the years and the different test campaigns.
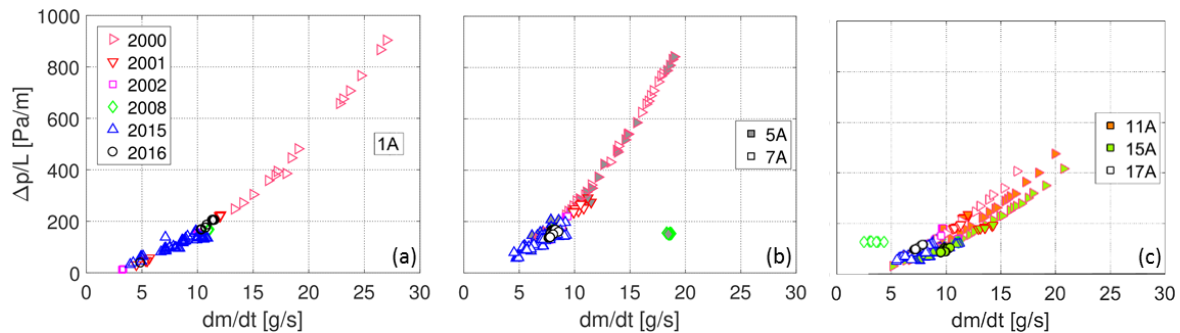
Figure 3. Measured hydraulic characteristic for (a) conductor 1A, (b) conductors 5A, 7A and (c) conductors 11A, 15A, 17A, respectively, in the different test campaigns.

To confirm the assessment of figure 3 and to look more in detail to the small differences therein, the data have been reduced to the pseudo-dimensionless quantities Re^* and f^*, directly related to the Reynolds number Re and friction factor f, respectively, as defined in Eqs. 1-2. The advantage of the pseudo-dimensionless form is that the effect of possible differences in the thermal-hydraulic conditions of the different points of the dataset is cancelled out.

$$Re^* = \frac{dm/dt}{\mu(p_{ave}, T_{ave})} \ [m] \tag{1}$$

$$f^* = \frac{2\rho(p_{ave}, T_{ave})}{4(dm/dt)^2} \frac{\Delta p}{L} \ [m^{-5}] \tag{2}$$

In Eqs. 1-2, dm/dt is the total mass flow rate, $\mu(p_{ave}, T_{ave})$ and $\rho(p_{ave}, T_{ave})$ are the viscosity and density, respectively, evaluated at mean (between inlet and outlet) pressure and temperature, while Δp is the pressure drop and L is the length of the conductor.

Figure 4 shows the pseudo-dimensionless hydraulic characteristic of the different conductors throughout the different experimental campaigns with the data from [5] used as a reference for the 2000 campaign and the associated error bar. The latter has been evaluated considering an error ~0.5% on pressure drop and ~6% on full scale (8 g/s) mass flow rate measurement, as from [7], together with the measurement error related to the oscillations of recorded traces.

The experimental data set for conductor 1A has been extended including not only the CSMC campaigns data, but also some specific results of the analysis of a short straight sample [1], [2], [4], see figure 4a. The dataset has been proven to be consistent as the $f^*(Re^*)$ of all the experimental points lays on the same trend line within the error bar. The data of the 2015 test campaign appear to be aligned more on a band than on a single line (true also for the other conductors), but note that re-calibrations of the flow meters were necessary during the test campaign due to some shift induced by the pressure rise.

Figure 4b highlights that the friction factor for the conductors with the spring is 60% higher than that of all the other conductors, as noted from the very beginning of the tests [5].

Figure 4c shows also that, even if OM conductors have nominally the same (bundle and hole) geometry, the f^* is quite different for the same values of Re^*. This is true in particular for the 15A conductor data measured in 2000, that present a much lower f^* with respect to the other instrumented conductors of the OM.
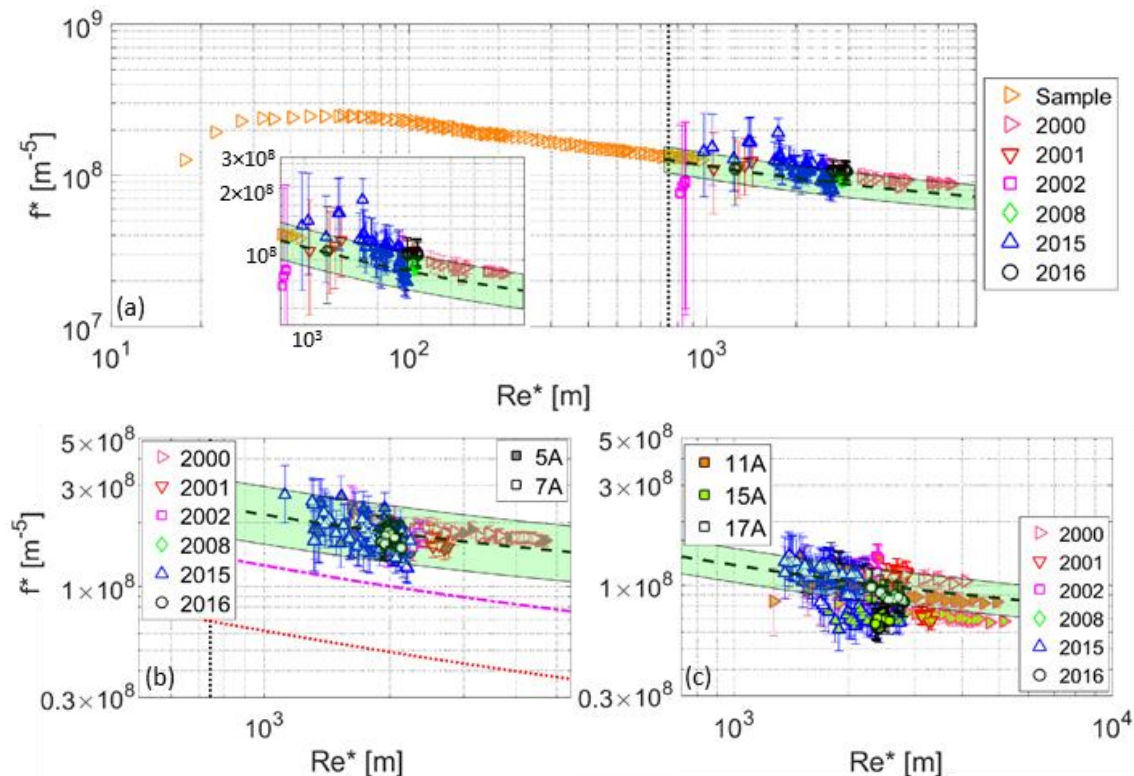
Figure 4. Total friction factor $f*(Re*)$ of conductors (a) 1A, (b) 5A, 7A and (c) 11A, 15A, 17A, respectively, for measurements from different test campaigns (symbols). In (a) and (c) the characteristic computed from available correlations for the hole and bundle regions are also reported (dashed lines), together with their error bar. In (b), the results of the combination of the bundle friction factor correlation from [1] with the correlations for the hole in Eq. 8 (dashed line), from [8] (dash-dotted line) and Eq. 6 and Eq. 9 from [9] (dotted line), respectively, are reported.

4. Accuracy of available correlations

4.1. Correlation for the bundle
A very general correlation for the bundle region of the CICC [1] is reported in Eqs. 3-5, in which the bundle region is treated as a porous medium due to the twisted and compact structure of the strands.

$$f_b = \frac{D_b^2 \varphi}{2K} \frac{1}{Re_b} + \frac{D_b \varphi^2}{2} \beta \left(\frac{D_b}{\varphi \sqrt{K}} \right)^{0.14} \frac{1}{Re_b^{0.14}} \tag{3}$$

$$K = 20.9 \cdot 10^{-9} \frac{\varphi^3}{(1-\varphi)^2} \ [m^2] \tag{4}$$

$$\beta = \frac{19.1}{\varphi^{4.23}} \ [m^{-1}] \tag{5}$$

where f_b is the friction factor in the bundle region, K is the permeability, Re_b is the bundle Reynolds number computed with the bundle hydraulic diameter and all other symbols have been defined in Table 1. Eqs. 3-5 apply with $Re_b < 10^5$.

4.2. Correlation for the hole

For all the conductors, except 5A and 7A, the central channel friction factor (f_h) can be computed according to [10] for a flat spiral with inner diameter of 10 mm and outer diameter of 12 mm. The friction factor is computed iteratively using Eq. 6-7 (valid for an hole Reynolds number $Re_h > 10^4$, where the characteristic length used in the Re_h definition is the inner diameter of the central channel):

$$h^+ = \left(\frac{h}{D_h}\right) \cdot Re_h \cdot \sqrt{\frac{f_h}{2}} \tag{6}$$

$$R(h^+) = 11.88 \cdot (h^+)^{0.039} \cdot \left(\frac{g}{h}\right)^{-0.299} = \sqrt{\frac{2}{f_h}} + 2.5 \cdot log\left(\frac{2h}{D_h}\right) + 3.75 \tag{7}$$

For conductors 5A and 7A, friction factor correlation for spring inserts in tubes [8] or helical-coiled-wire-inserted tubes [9] are available in literature. The correlation in [8] is given in the form of the friction factor in a smooth pipe with a proper multiplier N (valid for $Re_h < 10^5$), see Eq. 8.

$$f_h = 0.046 \cdot N \cdot Re^{-0.2} \text{ with } N = 2 \tag{8}$$

In [9], the friction factor is computed coupling Eq. 6 to a slightly different definition of $R(h^+)$, see Eq. 9, (valid for $Re_h < 10^5$):

$$R(h^+) = 7.0 \cdot (h^+)^{0.13}(\tan\alpha)^{-0.18} = \sqrt{\frac{2}{f_h}} + 2.5 \cdot log\left(\frac{2h}{D_h}\right) + 3.75 \tag{9}$$

4.3. Comparison of hydraulic characteristics resulting from correlations and measured data

The capability of the selected correlations to reproduce the measured $f^*(Re^*)$ is reported in figure 4 for all the conductors, while the hydraulic characteristic in dimensional form is shown in figure 5 for conductors 1A, 11A-15A-17A and in figure 6 for conductors 5A-7A, respectively.

For conductor 1A (figure 4a and figure 5a), the set of correlations adopted is able to reproduce the hydraulic behaviour of the conductor within the uncertainties of correlations and measurements with an average relative error of ±15% for $dm/d_{tot} > 3$ g/s. A similar picture is found for the conductors 11A, 15A and 17A, see figure 4c and figure 5b, with an average error of ~20% for $dm/dt_{tot} > 3$ g/s.

The available correlations largely underestimate the friction factor in conductors 5A and 7A, see figure 4b and figure 6a. Since the bundle correlation contributes to give a good agreement with the experimental data for all the other conductors, the problem must be hidden in the hole friction factor, which in fact is largely underestimated by the available correlations, see figure 6b. Note that the hole friction factor can be deduced from the experimental data evaluating the mass flow rate in the hole by difference, while the mass flow rate in the bundle is computed using the bundle friction factor correlation reported in Eqs. 3-5. The disagreement found here is to be attributed to the fact that the geometrical parameters of the spring used in 5A-8B conductors (see Table 1) are different from those used in [8] (thickness = 1.5 mm, gap = ~1.7 mm, pitch = ~3.3 mm) and [9] (thickness = 3 mm, gap = 7 mm, pitch = 10 mm) to develop the correlations.

To close this gap and for the sake of completeness assessing the hydraulic performance also of the layers of the CSMC featuring the spring, we develop here a correlation for the hole of conductors 5A-7A, based on the best fit of the experimental data in a power-law form, see Eq. 10.

$$f_h = A \cdot (Re_h)^C \tag{10}$$

The coefficients that best-fit the experimental data are $A = 5.09 \times 10^{-2}$ and $C = -6.31 \times 10^{-2}$, returning an agreement with measurements within ±19%.
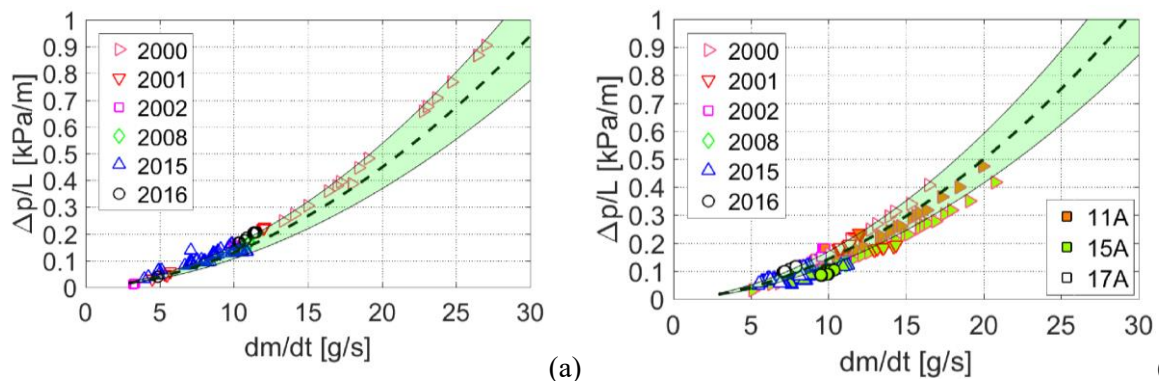
Figure 5. Hydraulic characteristic of conductors (a) 1A and (b) 11A, 15A and 17A, respectively, for measurements from different test campaigns. The computed characteristics from available correlations for the bundle and the hole, see text, are also reported (dashed line), together with their error bar.
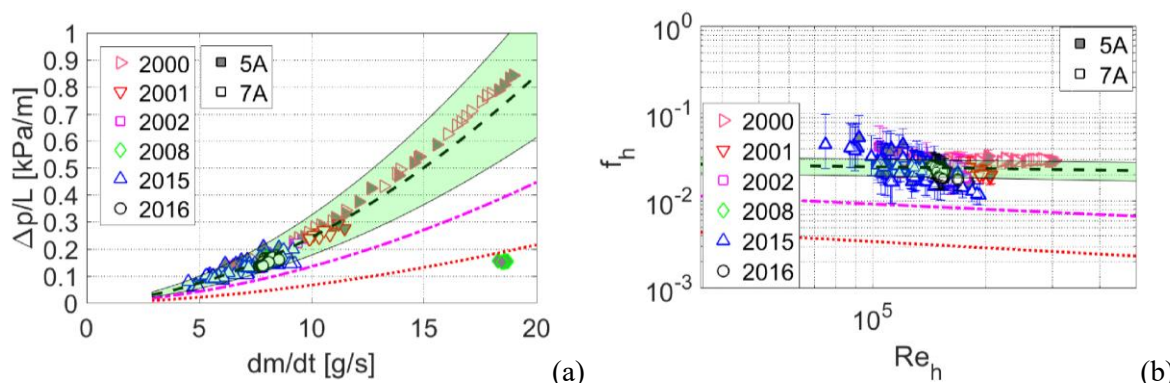
Figure 6. (a) Hydraulic characteristic and (b) friction factor $f_h(Re_h)$ in central channel for conductors 5A (solid symbols) and 7A (open symbols), for the different test campaigns. The results of the correlations in Eq. 10 (dashed line), in [8] (dash-dotted line) and in [9] (dotted line), respectively, are also reported in (b), while in (a) they are combined with the friction factor correlation from [1] for the bundle, to return the hydraulic characteristic of the conductor.
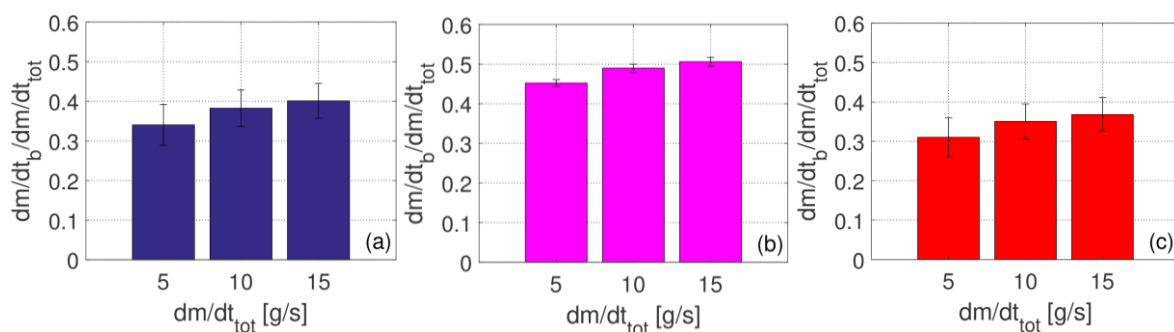
Figure 7. Ratio between bundle and total mass flow rate in different operating conditions for (a) 1A-4B, (b) 5A-8B conductors and (c) 9A-18B conductors.

4.4. Mass flow rate repartition

On the basis of the hydraulic characteristics computed above, it is possible to estimate the mass flow rate repartition between the hole and the bundle for the different conductors. The computed results show that the mass flow rate fraction in the bundle in the operating regime (5-15 g/s) is between 30% and 40% for the flat spiral conductors and around 45-50% for the spring conductors, see figure 7. The

higher fraction of the mass flow in the bundle of the coiled-wire conductors, if compared to the others, is payed at the cost of the larger pressure drop shown in figure 4.

5. Conclusions

In the present work, an overview of the hydraulic characteristic of the different types of CSMC conductors collected from different test campaigns has been presented, showing that no significant change is detected in the 15-years operation of the magnet.

Available correlations, widely used for the assessment of the ITER conductor performance, as well as for the design of the new generation of superconducting CICCs like those for future DEMO reactors, proved to be capable to reproduce the measured pressure drop with an accuracy better than 20% for the conductors where the hole is delimited with a flat spiral as in the ITER conductors or foreseen for instance for some options of the EU DEMO conductors [11].

For the conductors with the hole delimited by the coiled wire, available correlations demonstrated poor capability to reproduce the experimental data, and some ad-hoc recipe is required – however, conductors with the spring delimiting the hole are not under consideration for future machines in view of their larger hydraulic impedance if compared to the flat spiral option.

Finally, the computed results allow to estimate the mass flow rate repartition between the bundle and the hole, showing that the fraction of the mass flow rate in the bundle for the conductors with the spring is higher (45-50%) than that of the other conductors (30-40%) as expected from the larger impedance of the central channel in conductors 5A-8B.

References

[1]   Lewandowska M and Bagnasco M 2011 "Modified friction factor correlation for CICC's based on a porous media analogy" *Cryogenics* **51** pp. 541-545.
[2]   Zanino R and Savoldi Richard L 2006 "A review of thermal-hydraulic issues in ITER cable-in-conduit conductors" *Cryogenics* **46** pp. 541-555.
[3]   Tsuji H et al. 2001 "Progress of the ITER central solenoid model coil program" *Nucl. Fusion* **41** pp. 645-651.
[4]   Bruzzone P 2001 "Pressure drop and helium inlet in the ITER CS1 conductor" *Fus Eng Des.* **58-59** pp. 211-215.
[5]   Hamada K, Kato T, Kawano K, Hara E, Ando T, Tsuji H, Okuno K, Zanino R and Savoldi L 2002 "Experimental results of pressure drop measurements in ITER CS Model Coil tests" *Adv. Cryo. Eng.* **47** pp. 407-414.
[6]   Hamada K, Takahashi Y, Matsui K, Kato T and Okuno K 2004 "Effect of electromagnetic force on the pressure drop and coupling loss of a cable-in-conduit conductor" *Cryogenics* **44** pp. 45-52.
[7]   Isono T July 27 2016 Private communication.
[8]   Long A E June 1995 "Transverse heat transfer in a Cable-in-Conduit Conductor with Central Cooling Channel" MIT.
[9]   Sethumadhavan R and Raja Rao M 1983 "Turbolent flow heat transfer and fluid friction in helical-wire-coil-inserted tubes" *Int. J. Heat Mass Transfer* **26** (12) pp. 1833-1845.
[10]   Zanino R et al. 2000 "Friction factor correlation with Application to the Central channel of Cable-In-Conduit Super-Conductors for Fusion Magnets" *IEEE Trans. Appl. Supercond.* **10** (1) pp. 1066-1069.
[11]   Muzzi L et al. 2017 "Design, Manufacture, and Test of an 80 kA-Class Nb$_3$Sn Cable-In-Conduit Conductor With Rectangular Geometry and Distributed Pressure Relief Channels" *IEEE Trans. Appl. Supercond.* **27** (4) Art. ID. 4800206.